Journal of Quantitative Spectroscopy & Radiative Transfer 109 (2008) 2857–2868

Contents lists available at ScienceDirect

Journal of Quantitative Spectroscopy & Radiative Transfer

journal homepage: www.elsevier.com/locate/jqsrt

Oxygen, nitrogen and air broadening of HCN spectral lines at terahertz frequencies

Chun Yang [a], Jeanna Buldyreva [b], Iouli E. Gordon [c], François Rohart [d], Arnaud Cuisset [a], Gaël Mouret [a], Robin Bocquet [a], Francis Hindle [a,*]

[a] Laboratoire de Physico-Chimie de l'Atmosphère, UMR CNRS 8101, Université du Littoral Côte d'Opale, 189A Av. Maurice Schumann, 59140 Dunkerque, France
[b] Institut UTINAM, UMR CNRS 6213, Université de Franche-Comte, 16, Route de Gray, 25030 Besançon Cedex, France
[c] Harvard-Smithsonian Center for Astrophysics, Atomic and Molecular Physics Division, 60 Garden Street, Cambridge, MA 02138-1516, USA
[d] Laboratoire de Physique des Lasers, Atomes et Molécules, UMR CNRS 8523, Bâtiment P5-135, Université de Lille 1, 59655 Villeneuve d'Ascq Cedex, France

ARTICLE INFO

Article history:
Received 25 July 2008
Received in revised form
25 August 2008
Accepted 26 August 2008

Keywords:
HCN
Oxygen
Nitrogen
Broadening
Terahertz
Photomixing

ABSTRACT

The room-temperature nitrogen- and oxygen-broadening coefficients of hydrogen cyanide spectral lines have been measured in the 0.5–3 THz (17–100 cm^{-1}) frequency range (purely rotational transitions with $5 \leqslant J \leqslant 36$) by a continuous-wave terahertz spectrometer based on a photomixing source. An improved version of the Robert and Bonamy semiclassical formalism has been used to calculate the oxygen-broadening coefficients and resulted in a good agreement with these measurements. The nitrogen and oxygen data are combined to provide the air-broadening coefficients as used by the HITRAN database. A significant difference is observed between the measured and tabulated values for transitions with high values of the rotational quantum number. A new polynomial representation is suggested for inclusion in HITRAN. A similar polynomial expression has been derived for the nitrogen broadening to aid the studies of Titan's atmosphere.

1. Introduction

Hydrogen cyanide (HCN) is an important gas in astrophysical and atmospheric research. It is present in comets, interstellar clouds and the atmospheres of some planets and moons such as Titan for example [1,2]. Therefore, an extensive knowledge of its spectroscopic parameters is very important and they are tabulated in the major spectroscopic databases such as HITRAN [3]. The knowledge of HCN spectral parameters is also important for the star formation models as well as for industrial pollution monitoring and burning of bio-mass. The HCN line broadening by various foreign gases is of particular interest. For example, the values of the foreign gas broadening parameters can be used to estimate temperatures and concentrations of the gas in different astrophysical objects [4]. There have been extensive experimental studies of these broadening parameters in the infrared region for air and N_2 perturbation [5–8] and references therein. The terahertz (THz) region has been studied far less extensively and only the N_2-broadening parameters have been measured using a far-infrared Fourier spectrometer [9]. The O_2-broadening data in any spectral region are very limited. The purpose of the experiments described in this paper is to extend the available oxygen-broadening information. The N_2-broadened coefficients have also been measured allowing the air-broadening coefficients to be determined.

* Corresponding author.
E-mail address: francis.hindle@univ-littoral.fr (F. Hindle).

0022-4073/$ - see front matter © 2008 Elsevier Ltd. All rights reserved.
doi:10.1016/j.jqsrt.2008.08.005

Computations of collisional broadening coefficients for HCN–N_2 system are currently available for (0,1,0) band at room [10] and low [11] temperatures in the framework of the traditional Robert and Bonamy (RB) semiclassical approach with parabolic trajectories for the relative molecular motion [12]. Recently, the room-temperature coefficients had been also evaluated [13] by the improved version of the RB formalism [14] involving the exact solutions of the classical equations of motion [15] (RBE). In contrast, the oxygen-broadening coefficients for HCN (vib)rotational lines to our knowledge have never been computed. We present therefore their theoretical values by the semiclassical RBE approach. Since for the case of two linear molecules this approach had been already discussed in detail elsewhere [14], in Section 4 we briefly present its key features and main formulae relative to the linewidth calculation. The numerical results are given and compared with the experimental data in Section 5. In Section 6, the air-broadening coefficients deduced from the measured data are compared to existing infrared data and are used to determine a new polynomial function which is suggested for inclusion in HITRAN as it extends to higher rotational levels.

2. Experimental procedure

The use of ultra-fast electronic components and optical heterodyning or "photomixing" can provide access to frequencies from 0.1 to 3 THz (3.3–100 cm^{-1}). Photomixing [16] is a frequency down-conversion technique where two lasers close in frequency are used to create a beatnote at the target frequency. A semiconductor material with a suitably short carrier lifetime is employed to convert the beatnote into an electrical current which is subsequently radiated by an antenna. Photomixing sources have already demonstrated their utility for the spectroscopy of gases [17–20] along with the quantitative analysis of complex samples such as cigarette smoke containing many chemical species and a high degree of aerosols [21].

A continuous-wave terahertz (CW-THz) spectrometer was constructed using a photomixing radiation source, Fig. 1. The instrument can be divided into the following functional units: a dual-frequency optical source, the photomixer element, a THz beam propagation path including the sample cell and a detector (bolometer). The optical source contains two (Toptica DL-100) extended cavity diode lasers (ECDL) operating at 780 nm. The lasers are spatially mixed using a beam splitter to create a beatnote in the THz frequency range. In order to optimize the spectral resolution of the source, a frequency stabilization scheme was applied to each laser. The first laser was frequency locked to a saturated absorption feature of the rubidium D_2-line, using commercially available apparatus (TEM Messtechnik, CoSy). The second laser was stabilized using a low-contrast Fabry–Pérot interferometer system (TEM Messtechnik, iScan). Unlike many Fabry–Pérot systems that can only provide information at the resonant frequency, the advantage of this low-contrast interferometer is that it is capable of providing a stabilization signal at any frequency. An error signal generated by the difference between an arbitrary set-point and the Fabry–Pérot is applied to the peizoelectic element of the laser. Hence the laser can be frequency scanned across its gain profile with an active frequency correction being provided by the interferometer. In the particular case of an ECDL, the fine adjustment of the grating alignment using the piezoelectric allows a continuous tuning range of around 10 GHz to be routinely obtained. Larger frequency steps are realized by manual adjustments of the grating alignment along with current and temperature of the laser diode. A tapered semiconductor optical amplifier (Toptica, BoosTA) was used to increase available power of the dual-frequency source up to 1.5 W. To verify the correct operation and stabilization of the lasers and

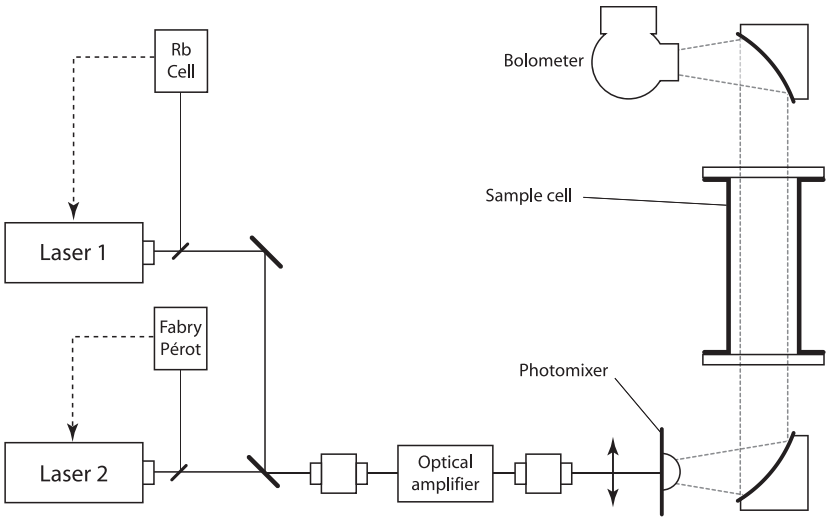

Fig. 1. CW-THz spectrometer composed an optical source, the photomixer element, THz beam propagation path and bolometer. Optical isolators are placed at the entry and exit of the amplifier.

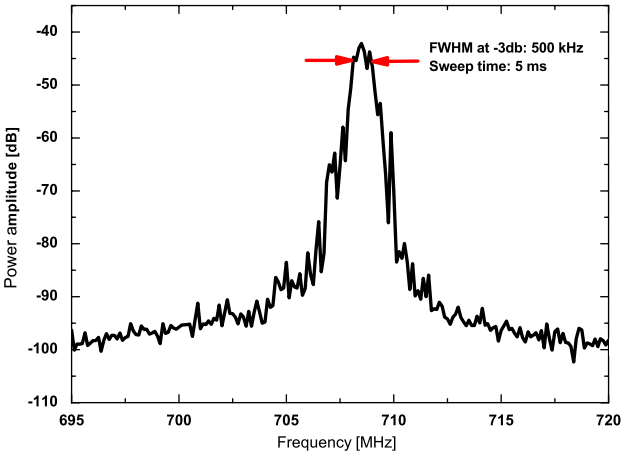

Fig. 2. Beatnote between two ECDL, measured at the exit of the tapered amplifier with a sweep time of 5 ms.

the amplifier, a microwave beatnote was measured using a fast photodiode and a spectrum analyzer, Fig. 2. The spectral purity of the beatnote was determined to be 0.5 MHz at −3 dB.

The photomixing elements were fabricated by the Institut d'Electronique de Microélectronique et de Nanotechnologie (IEMN, Lille, France). They consist of a GaAs substrate with a 1 μm layer of low-temperature grown GaAs (LTG-GaAs) deposited by molecular beam epitaxy at a temperature of 300 °C. An electrode array and the radiating antenna are patterned on the device surface using electron beam lithography. The electrode array has a dimension of 8 μm × 8 μm and consists of 5 interdigitated electrodes each of 0.2 μm width. The electrode array is located at the center of a pair of log spiral antenna. The dual-frequency laser beam is focused onto the center of the electrode array to which a voltage V_{BIAS} is applied. The LTG-GaAs has a sufficiently short carrier lifetime in order to conserve the difference frequency of the THz beatnote; hence, a corresponding current i_{THz} is created. The current is coupled to the broadband spiral antenna radiating a THz electromagnetic wave. This device is capable of producing up to 100 nW of THz radiation and operating at frequencies between 0.1 and 3 THz. The highly divergent THz beam produced by the photomixer is collimated by a combination of a hemispherical silicon lens placed on the device substrate and a metal off-axis parabolic mirror. The collimated beam passes through a sample chamber of length 104 mm by means of two Teflon windows before being focused onto the detector by a second parabolic mirror. The detector used is a silicon bolometer operating at 4.2 K and having a noise equivalent power of 2.0×10^{-12} W/Hz$^{1/2}$.

Gaseous HCN was produced by reacting potassium cyanide with phosphoric acid. Due to the strong permanent dipole moment of HCN which results in particularly intense rotational transitions, a small quantity, typically 0.02 mbar, of HCN was introduced into the sample chamber and subsequently diluted with either nitrogen or oxygen. Resulting maximum observed absorptions remained smaller than 90%. Spectra were recorded for the ground-state $(0,0,0)$ and upper degenerated-state $(0,1^1_2,0)$ HCN transitions in the frequency range of 0.53–3.26 THz ($J = 5$ to 36). An instrument background recorded under identical conditions accompanies each measured spectra, as illustrated in Fig. 3. The oscillations present in the data are caused by a Fabry–Pérot effect established between the photomixer and the bolometer. The periodicity corresponds to the total length of the THz propagation path of 81 cm. For each transition examined, a minimum of 15 independent spectra were recorded covering pressures up to 40 mbar.

3. Results and data analysis

The measured spectra were normalized by an instrument background and fitted, taking account of the Beer–Lambert law, to a Voigt profile based on the complex probability function [22] by a non-linear minimization routine. Typical normalized data are presented in Fig. 4 showing the broadening of HCN by oxygen. The Doppler contribution was calculated for each transition, while the collisional broadening $\Delta\upsilon_{HWHM}$, integrated line intensity area and center frequency were minimized for each recorded spectrum. The collisional broadening was determined for both oxygen and nitrogen as a function of pressure up to total pressures of 40 mbar.

The broadening coefficients γ_{HCN-O_2} and γ_{HCN-N_2} were determined by the linear regression of these data for each transition and are presented in Tables 1 and 2. An example is presented in Fig. 5 for the oxygen broadening of the line corresponding to the transition $J = 22 \leftarrow 21$ at 1946.2 GHz where the calculated Doppler broadening HWHM is 2.3 MHz. As expected, the oxygen- and nitrogen-broadening coefficients decrease with increasing J, Fig. 6, and the interaction with nitrogen is approximately 1.7 times stronger than for oxygen. The correct operation of the spectrometer was confirmed by comparison of the nitrogen-broadening results with those previously published by Sergent-Rozey et al. [9], Table 1. For the majority of the lines, the difference between these data sets is commensurate with the measurement uncertainties.

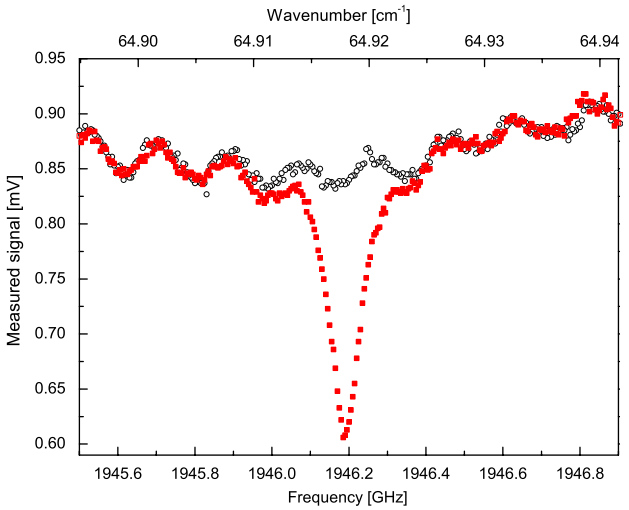

Fig. 3. Observed spectrum of 0.02 mbar of HCN diluted in oxygen, total pressure 24.2 mbar (filled squares), for the transition $J = 22 \leftarrow 21$. Instrument background (open circles). $T = 294$ K.

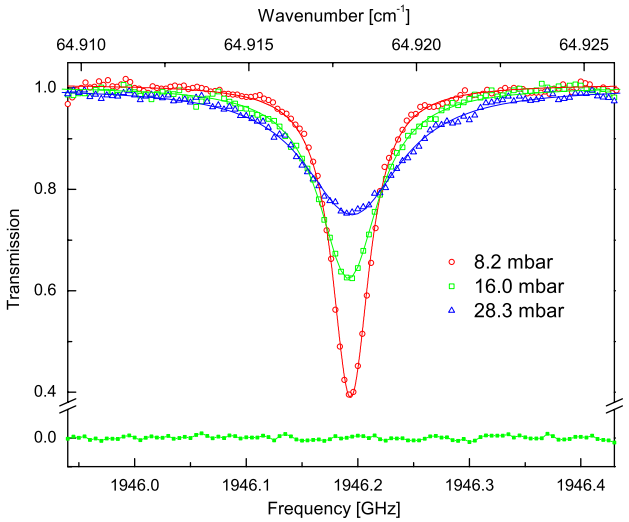

Fig. 4. Observed transmission spectra for HCN and oxygen mixtures, for the transition $J = 22 \leftarrow 21$. The HCN partial pressure was 0.02 mbar, the total pressures after dilution with oxygen were (circles) 8.2 mbar, (squares) 16.0 mbar and (triangles) 28.3 mbar. Spectra are shown with a fitted Voigt absorption profile (solid lines), the residual for the spectra at 28.3 mbar is also shown. $T = 294$ K.

4. Theoretical study of oxygen-broadening coefficients

In the simplest case of linear active molecule perturbed by a diatom, the HWHM of a spectral line corresponding to the optical (radiative) transition $f \leftarrow i$ is given in the framework of the RB formalism [12] by

$$\gamma_{fi} = n\langle v[1 - e^{-Re\, S_2}]\rangle_{b,v,J_2} \tag{1}$$

where n is the number density of perturbers and the averaging is made over the relative velocity of colliding molecules v, the impact parameter b and the rotational quantum number of the perturbing molecule J_2. Instead of the averaging with the Maxwell–Boltzmann distribution for the relative velocities, the mean thermal velocity is traditionally used: $\bar{v} = [8k_B T/(\pi m)]^{1/2}$, where k_B is the Boltzmann constant, T is the temperature in Kelvin and m is the reduced mass of the colliding pair. The quantity S_2 represents the second-order contribution (proportional to the second power of the anisotropic interaction potential) to the scattering matrix S which is detailed in [12] and can be specified for the RBE approach as soon as the interaction potential and the trajectory model are chosen.

Table 1
HCN–nitrogen broadening coefficients for transitions $J+1 \leftarrow J$

J	Frequency (GHz)	Ground state γ_{HCN-N_2} $(0,0,0)$ This work (MHz/mbar)	Ground state γ_{HCN-N_2} $(0,0,0)$ [9] (MHz/mbar)	Frequency (GHz)	Upper degenerated state γ_{HCN-N_2} $(0,0^1_2,0)$ This work (MHz/mbar)
5	531.7	4.07(4)			
6	620.3	3.80(8)	3.78(14)		
7	708.9	3.17(5)	3.62(12)	712.4	4.12(7)
8	797.4	3.58(4)	3.38(17)	801.4	3.58(4)
9	886.0	3.35(4)	3.48(13)	890.3	3.40(5)
10	974.5	3.39(4)	3.30(16)	979.3	3.63(5)
11	1063.0	3.35(4)	3.39(11)	1068.2	3.40(4)
12	1151.5	3.47(5)	3.37(13)	1157.1	3.67(7)
13	1239.9	3.20(2)	3.37(10)	1246.0	3.08(3)
14	1328.3	2.90(1)	3.21(9)		
16	1505.0	3.06(3)	3.18(11)		
17	1593.3	3.27(2)	3.25(10)		
19	1769.9	3.18(2)	3.09(14)		
20	1858.0	3.21(3)	3.23(15)		
21	1946.2	2.97(2)	3.10(12)		
22	2034.3	3.20(4)	3.00(14)		
23	2122.4	3.16(2)	3.01(14)		
24	2210.4	3.06(4)	2.97(15)		
25	2298.3	2.84(3)	2.72(16)		
28	2561.8	2.84(3)	2.84(14)		
30	2737.2	2.79(2)	2.67(16)		
31	2842.8	2.81(2)	2.41(16)		
32	2912.3	2.46(3)	2.25(17)		
34	3087.2	2.19(5)			

For HCN interacting with a homonuclear diatomic molecule, the electrostatic forces are the most important and yield the totality of the linewidth value [11,13], except the very low values of the rotational quantum number for which the short-range terms give an additional contribution. In a similar manner, we suppose that for the HCN–O_2 system the anisotropic part of the interaction potential can be modeled as

$$V_{\text{aniso}} = V_{\mu_1 Q_2} + V_{Q_1 Q_2} + 4\varepsilon\gamma_1 \left[\left(\frac{\sigma}{r}\right)^{12} - \left(\frac{\sigma}{r}\right)^{6} \right] P_2(\cos\,\theta) \tag{2}$$

In this equation the long-range electrostatic dipole–quadrupole and quadrupole–quadrupole interactions are completed by a Lennard–Jones function with usual parameters ε and σ which is multiplied by the polarizability anisotropy of HCN $\gamma_1 = 0.257$ [11] and the Legendre polynomial P_2 in order to account for the angular dependence of the short-range forces. Since the multipole moments of the interacting molecules are quite well known, for all computations we fixed their values to $\mu_1 = 2.963$ D for the $(0,0,0)$ ground state and $\mu_1 = 2.915$ D for the $(0,1,0)$ vibrational state of HCN [23] as well as to $Q_1 = 3.10$ DÅ [24] and $Q_2 = -0.39$ DÅ [25]. The Lennard–Jones parameters were calculated by the usual combinations rules using $\varepsilon_{HCN} = 569.1$ K, $\sigma_{HCN} = 3.63$ Å [26] and $\varepsilon_{O_2} = 113$ K, $\sigma_{O_2} = 3.433$ [27], so that $\varepsilon = 253.6$ K and $\sigma = 3.532$ Å. In contrast with the HCN–N_2 case (where the electrostatic contributions in the linewidth are clearly dominant even for very small values of the rotational quantum number), the short-range forces contribution for HCN–O_2 is quite important at small J and can be adjusted to fit better the experimental values, as it is shown below. To employ the model of exact trajectories, the interaction potential (2) must be put in the form invariant under overall rotations of the system:

$$V_{\text{aniso}}(\vec{r}) = \sum_{l_1 l_2 l} V_{l_1 l_2 l}(r) \sum_{m_1 m_2 m} C^{lm}_{l_1 m_1 l_2 m_2} Y_{l_1 m_1}(\theta_1, \varphi_1) Y_{l_2 m_2}(\theta_2, \varphi_2) C^{*}_{lm}(\theta, \varphi) \tag{3}$$

This expansion into a series of three spherical harmonics tied to the orientations of both molecular axes ($Y_{l_1 m_1}, Y_{l_2 m_2}$) and the intermolecular distance vector $\vec{r}$ ($C_{lm}(\theta,\varphi) = [4\pi/(2l+1)]^{1/2} Y_{lm}(\theta,\varphi)$) in the laboratory-fixed frame enables the separation of the angular (spherical harmonics) and radial ($V_{l_1 l_2 l}(r)$) dependences of the interaction potential energy. The asterisk stands for the complex conjugation and $C^{lm}_{l_1 m_1 l_2 m_2}$ is the Clebsch–Gordan coefficient. For the three terms of (2) the corresponding radial components read

$$V_{123}(r) = 4\pi \frac{\mu_1 Q_2}{r^4} \quad V_{224}(r) = \frac{4\pi\sqrt{70}}{5} \frac{Q_1 Q_2}{r^5} \quad V_{202}(r) = \frac{4\pi}{5} 4\varepsilon\gamma_1 \left[\left(\frac{\sigma}{r}\right)^{12} - \left(\frac{\sigma}{r}\right)^{6} \right] \tag{4}$$

Table 2
HCN–oxygen broadening coefficients for transitions $J+1 \leftarrow J$

J	Frequency (GHz)	Ground state γ_{HCN-O_2} $(0,0,0)$ This work (MHz/mbar)	Theory Viso1 (MHz/mbar)	Frequency (GHz)	Upper degenerated state γ_{HCN-O_2} $(0,0^1_2,0)$ This work (MHz/mbar)	Theory Viso1 (MHz/mbar)
0			2.54			2.52
1			2.53			2.50
2			2.51			2.49
3			2.49			2.46
4			2.43			2.41
5	531.7	2.11(2)	2.36			2.33
6	620.3	2.29(1)	2.27			2.25
7	708.9	2.10(5)	2.20			2.17
8	797.4	2.05(2)	2.13	801.4	2.38(3)	2.11
9	886.0	2.18(2)	2.09	890.3	2.12(3)	2.06
10	974.5	2.22(3)	2.05	979.3	2.05(3)	2.02
11	1063.0	2.17(1)	2.02	1068.2	2.02(2)	1.99
12	1151.5	2.13(2)	2.00	1157.1	2.08(5)	1.97
13	1239.9	1.90(1)	1.98	1246.0	1.94(2)	1.96
14	1328.3	1.92(2)	1.97			1.94
16	1505.0	1.85(1)	1.96			1.93
17	1593.3	2.02(2)	1.95			1.92
19	1769.9	1.91(1)	1.93			1.91
20	1858.0	2.03(1)	1.91			1.89
21	1946.2	1.67(2)	1.89			1.86
22	2034.3	1.81(2)	1.86			1.83
23	2122.4	1.81(1)	1.83			1.80
24	2210.4	1.68(1)	1.79			1.76
25	2298.3	1.62(1)	1.75			1.72
28	2561.8	1.54(1)	1.70			1.67
30	2737.2	1.52(2)	1.65			1.61
31	2842.8	1.65(1)	1.59			1.56
32	2912.3	1.62(2)	1.53			1.50
34	3087.2	1.43(2)	1.47			1.44
36	3261.7	1.23(4)	1.41			1.38
37			1.34			1.31
38			1.28			1.25
39			1.21			1.18
40			1.15			1.12
41			1.08			1.05
42			1.02			0.99

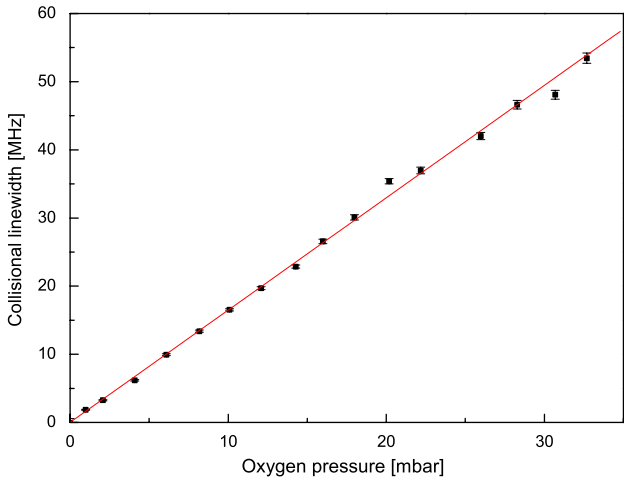

Fig. 5. Collisional linewidths as a function of pressure for the transition $J = 22 \leftarrow 21$. A weighted least-squares fit provides a broadening coefficient of 1.65 ± 0.01 MHz/mbar. $T = 294$ K.

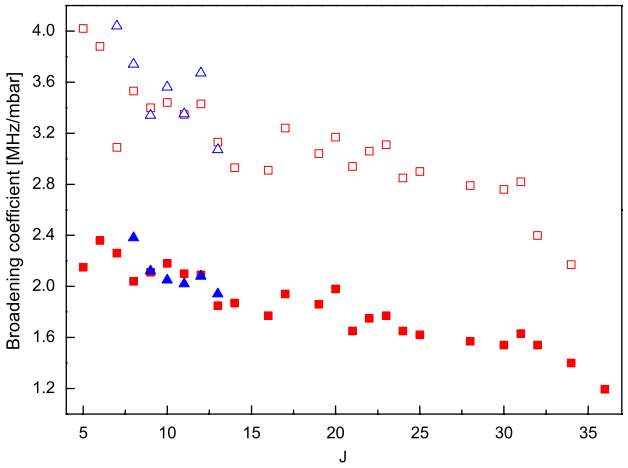

Fig. 6. Oxygen- (filled symbols) and nitrogen- (open symbols) broadening coefficients for the $J{+}1 \leftarrow J$ ground-state transitions (squares) and upper degenerated-state transitions (triangles) at $T = 294$ K. The error bars of the broadening coefficients are smaller or equal to the size of the symbols used.

These radial components are computed numerically for r varying from the minimal distance of the closest approach $r_{c\,min}$ (defined by the relative velocity v and the isotropic potential parameters) to 13 Å (where the contributions to the linewidth become negligible).

The second-order contribution S_2 is then given by

$$S_2 = 2\hbar^{-2}\left(\frac{r_c}{v}\right)^2 \sum_{l_1 l_2 l}\left[\sum_{j_i' j_2'}\left(C^{j_i' 0}_{j_i 0 l_1 0}\right)^2\left(C^{j_2' 0}_{j_2 0 l_2 0}\right)^2 f_{l_1 l_2 l} + \sum_{j_f' j_2'}\left(C^{j_f' 0}_{j_f 0 l_1 0}\right)^2\left(C^{j_2' 0}_{j_2 0 l_2 0}\right)^2 f_{l_1 l_2 l} - \sum_{j_2'}(-1)^{j_2+j_2'}\left(C^{j_2' 0}_{j_2 0 l_2 0}\right)^2 D^{(l_1)}_{j_i j_f} f_{l_1 l_2 l}\right] \tag{5}$$

where the primed rotational numbers stand for the states induced by collision $D^{(l_1)}_{j_i j_f} = 2(-1)^{j_i+j_f}[(2j_i+1)(2j_f+1)]^{1/2} C^{j_i}_{j_i 0 l_1 0} C^{j_f}_{j_f 0 l_1 0} W(j_i j_f j_i j_f; 1 l_1)$ with $W(j_i j_f j_i j_f; 1 l_1)$ denoting the Racah coefficient, and $f_{l_1 l_2 l}(r_c, k_c)$ is the so-called resonance function defined by the distance of the closest approach r_c (for a given value of the impact parameter b) and the resonance parameter $k_c = \omega r_c/v$ (the frequency $\omega = \omega_{ii'} + \omega_{22'}$ characterizes how close are the pairs of states ii' and $22'$ to the exact resonance):

$$f_{l_1 l_2 l}(r_c, k_c) = \sum_m \frac{(l-m)!(l+m)!}{2^{2l}((l-m)/2)!^2((l+m)/2)!^2}\left\{\int_1^{y_{max}} \frac{dy V_{l_1 l_2 l}(r_c y) y \cos\left[k_c A_0(y) + m\sqrt{1 - V^*_{iso}(r_c)} A_2(y)\right]}{\sqrt{y^2 - 1 + V^*_{iso}(r_c) - y^2 V^*_{iso}(r_c y)}}\right\}^2,$$

$$A_n(y) = \int_1^y \frac{dz}{z^{n-1}\sqrt{z^2 - 1 + V^*_{iso}(r_c) - z^2 V^*_{iso}(r_c z)}} \tag{6}$$

In contrast with the resonance functions of the Anderson–Tsao–Curnutte theory [28] (which are tabulated for the long-range interactions) or those of the RB formalism with parabolic trajectories [12] (which are expressed analytically through the Bessel functions), the exact-trajectory resonance functions, (6), are computed by a numerical integration over the reduced trajectory parameter $y \equiv r/r_c$ and depend on the reduced isotropic potential $V^*_{iso} = 2V_{iso}/(mv^2)$ which governs the relative molecular motion.

The parameters of V_{iso} approximated as usual by a Lennard–Jones function $V_{iso} = 4\varepsilon\left|(\sigma/r)^{12} - (\sigma/r)^6\right|$ influence greatly the resonance functions and, consequently, the linewidth computation. We analyze below various V_{iso} parameterizations available for HCN–O_2.

The calculation of the resonance parameter k_c corresponding to the simultaneous collisional transitions in the active and perturbing molecules needs the rotational constant values for the active molecule in the ground state or degenerated vibrational state (only pure rotational radiative transitions are considered here) as well as for the perturbing molecule in the ground state (collisions are supposed to induce only rotational transitions). For HCN we took $B_0 = 44.315909$ GHz for the ground and $B_1 = 44.534538$ GHz for the degenerated vibrational states [29]. For O_2 $B_0 = 43.103110$ GHz calculated with B_e and α_e of Herzberg [30] was used.

5. Analysis of isotropic potential parameterization and comparison with experimental data

The oxygen-broadening coefficients were computed for the ground state $(0,0,0)$ using the isotropic potential Lennard–Jones parameters $\varepsilon = 95.854$ K, $\sigma = 3.676$ Å (obtained by the combination rules with $\varepsilon_{HCN} = 81.31$ K, $\sigma_{HCN} = 3.918$ Å, as recommended in [11], and $\varepsilon_{O_2} = 113$ K, $\sigma_{O_2} = 3.433$ [27], as for the anisotropic potential component V_{202}).

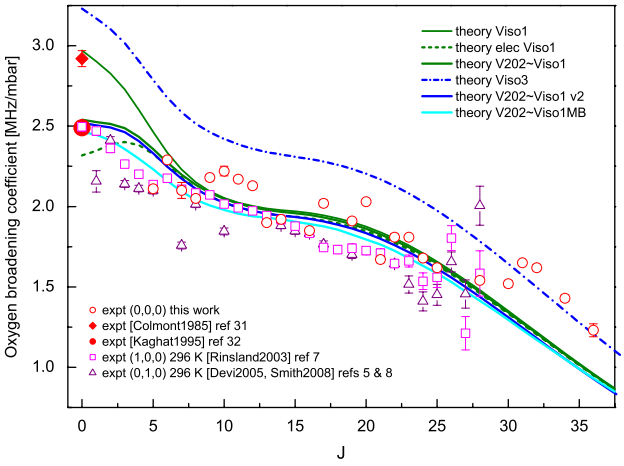

Fig. 7. Comparison of theoretical and experimental dependences of HCN–O_2 broadening coefficients on the rotational quantum number at 294 K. Experimental data for (1, 0, 0) $R(J)$ lines are calculated from the nitrogen- and air-broadening data [1]; for (0, 1, 0) $R(J)$ lines they are obtained from the measurements of [2] (air-broadening) and [3] (nitrogen-broadening).

The results are plotted on Fig. 7 (theoretical curves "Viso1") together with the experimental data of the present work and the measurements of Colmont [31] and Kaghat [32] for the rotational transition $J = 1 \leftarrow 0$. Since, at present, no apparent vibrational dependence has been observed for the HCN-broadening coefficients [3], in order to extend the comparison to small values of the rotational quantum number we plotted on the same figure the broadening coefficients estimated from the measurements of Rinsland et al. [7] for the (1, 0, 0) $R(J)$ lines of air- and N_2-perturbed HCN at 296 K as well as from the measurements of Devi et al. [5] (air-perturbed) and those of Smith et al. [8] (nitrogen-broadened) (0, 1, 0) $R(J)$ lines at 296 K. The oxygen broadening was estimated using the common equation

$$\gamma_{\text{air}} = 0.79\gamma_{N_2} + 0.21\gamma_{O_2} \tag{7}$$

As can be seen from this figure, the chosen V_{iso} parameterization leads to a very good agreement with the measurements. The dominant character of the electrostatic interactions (curve "elec Viso1") for middle and high values of J is also demonstrated. The agreement with (1, 0, 0) experimental data for very low J can be further improved by changing the Lennard–Jones parameters in the V_{202} term of the anisotropic potential. Indeed, taking $\varepsilon = 95.854$ K and $\sigma = 3.676$ Å (the same parameter values as for V_{iso}) reduces the contribution of the component V_{202} in the linewidth (thick solid line "V202~Viso1" in Fig. 7).

It is also noted that the slight overestimation of the broadening coefficient for small J values ($J = 1$–6) can be attributed to the use of the mean thermal velocity in our computations. Indeed, it has been shown for HCN–N_2 [13] that the Maxwell averaging even with three values of v ($0.5\bar{v}$, $\bar{v}$ and $1.5\bar{v}$) enables a more realistic decreasing of the theoretical RBE linewidths for the small values of the rotational quantum number. The analogous computation for HCN–O_2 ("MB" curve in Fig. 7) confirms this explication. The somewhat low values of the theoretical broadening coefficient for high values of J initiated us to test other possible parameters for the isotropic potential. Since the multipole moments were fixed in our computations and only the electrostatic contributions are responsible for the high J value linewidths, solely the V_{iso} potential can be modified to improve the fit of the experimental data. An alternative set of Lennard–Jones parameters for O_2 molecule ($\varepsilon_{O_2} = 88$ K, $\sigma_{O_2} = 3.541$) [33] resulted in slightly different parameters for HCN–O_2: $\varepsilon = 84.85$ K, $\sigma = 3.730$ Å, but no significant change was observed for the computed linewidths. We made therefore one more computation taking this time a deeper HCN isotropic potential [26], so that the Lennard–Jones parameters for the anisotropic V_{202} term and the isotropic potential were exactly the same. The resulting theoretical curve ("Viso3") in Fig. 7 reproduces very well the broadening coefficients for high J values but obviously overestimates the linewidths at middle and small J. As it had already been performed previously [11], we did not test the Lennard–Jones N-6 or spherical average of the atom–atom interactions models for the isotropic potential, since no significant difference between the broadening coefficients obtained by these and the usual 12–6 Lennard–Jones form was stated by the authors. For HCN–O_2 we retained therefore the Viso1 parameterization of the isotropic potential as the most appropriate, Table 2. The best parameterization for the anisotropic potential component V_{202} appears to have the same values of ε and σ as Viso1.

For the rotational transitions referring to the $(0, 1\frac{1}{2}, 0)$ vibrational state (the rotational constant value and the dipolar moment of HCN change as mentioned at the end of Section 4), the theoretical curve is practically indistinguishable from that of the (0, 0, 0) ground state (thick dashed line in Fig. 7). The corresponding numerical values are presented in Table 2. This is less clear for the experimental data where the measurement uncertainty does not allow the vibrational dependency to be excluded.

6. Air-broadened half-widths

The air-broadened half-widths in the pure rotational band were estimated from our oxygen- and nitrogen-broadening data using (7). These values are shown in Fig. 8 along with the polynomial (dashed line) that was used to estimate the values for all the bands of HCN in the HITRAN2004 database [3]. The polynomial was derived from the fit to the experimental data from the (1,0,0) and (0,2,0) bands [6,7]. The polynomial was used for $|m| \leqslant 29$, where $m = -J''$ for the P branches and $m = J'$ for R-branches. For $|m| > 29$ the constant value of 0.088 cm^{-1} atm^{-1} was used (the horizontal dashed-dotted line in Fig. 8) due to lack of the experimental information for higher J-values.

It is obvious that the value of 0.088 cm^{-1} atm^{-1} significantly overestimates the air-broadened half-widths for higher J transitions measured in this work. In Fig. 8 the data from P and R branches of (1,0,0) and (0,1,0) bands [5,7] are also shown. They were fitted together with the values from this work to obtain a fourth-order polynomial

$$\gamma_{air} = A_0 + A_1|m| + A_2|m|^2 + A_3|m|^3 + A_4|m|^4 \quad (8)$$

The values from the (0,2,0) band [6] were not included in the fit as they are very close to the values from (1,0,0) band which is also a parallel band. The results of the fit are given in Table 3. The new polynomial is suggested for the new edition of the HITRAN database, because it takes into account values for the higher J transitions and also derived from both parallel and perpendicular bands. Although the fitting data were only available for $|m| \leqslant 34$, it appears that the polynomial follows the trend up to $|m| = 40$; therefore, it seems to be safe to use for $|m| \leqslant 40$, with HITRAN uncertainty code 5 (5–10%) [3]. For $|m| > 40$ it is suggested to use the polynomial value for $|m| = 40$ until more data become available. The HCN-broadening parameters are currently used to study the atmospheric composition of Titan; it is therefore important to have a similar polynomial expression for the nitrogen-broadening coefficient. Such an expression was derived in [8] and it is interesting to see if it can be improved by utilizing the high J data from this work. Data for the (1,0,0) band [7], the (0,1,0) band [8,11,34] and the pure rotation band of this work and [13,31] were together fitted to a third-order polynomial analogous to (8). The results are shown in Fig. 9. Apart from the polynomial derived in this work (the coefficients are also given in Table 3), the polynomial function from [8] is also plotted. Interestingly, it also follows the data very well even at higher $|m|$ values.

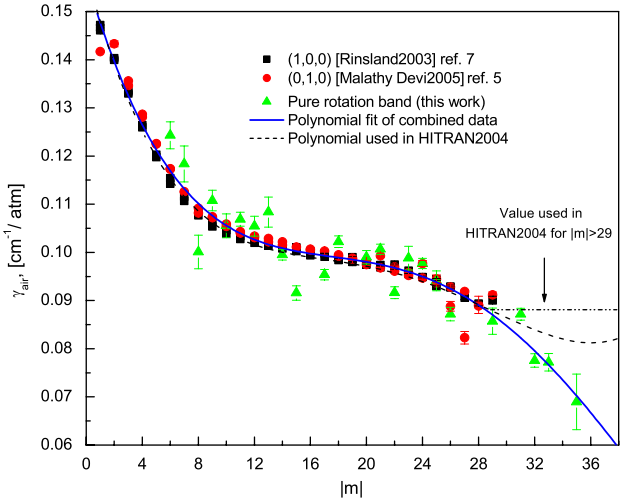

Fig. 8. Air-broadened half-widths of HCN from pure rotational, (1,0,0) and (0,1,0) bands.

Table 3
Fourth-order polynomial fit (Eq. (8) to experimental air and nitrogen broadened half-widths)

Parameter	Value (air) All bands	Error (air)	Value (N_2) All bands	Error (N_2)
A_0	0.15694	1.4×10^{-3}	0.17396	1.1×10^{-3}
A_1	-9.86×10^{-3}	5.0×10^{-4}	−0.00997	2.7×10^{-4}
A_2	6.29144×10^{-4}	$5.\ 7 \times 10^{-5}$	5.039×10^{-4}	1.8×10^{-5}
A_3	-1.71209×10^{-5}	2.4×10^{-6}	-8.58211×10^{-6}	3.5×10^{-7}
A_4	1.47824×10^{-7}	3.5×10^{-8}		
R^2	0.97205		0.96844	
St. dev.	0.0024		0.00313	
N points	133		161	

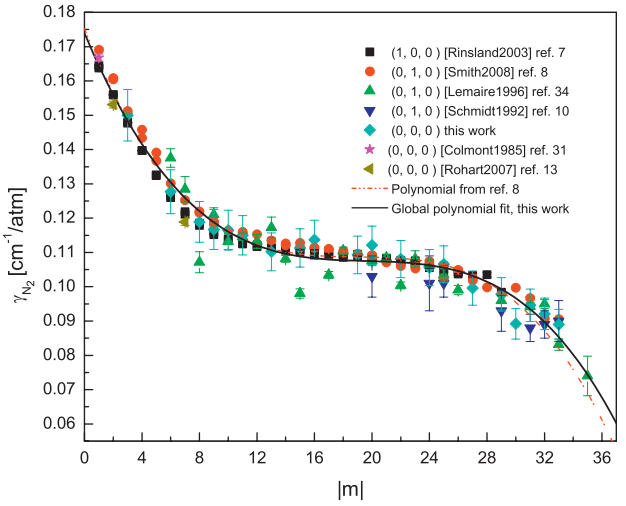

Fig. 9. N_2-broadened half-widths of HCN from pure rotational, $(1,0,0)$ and $(0,1,0)$ bands.

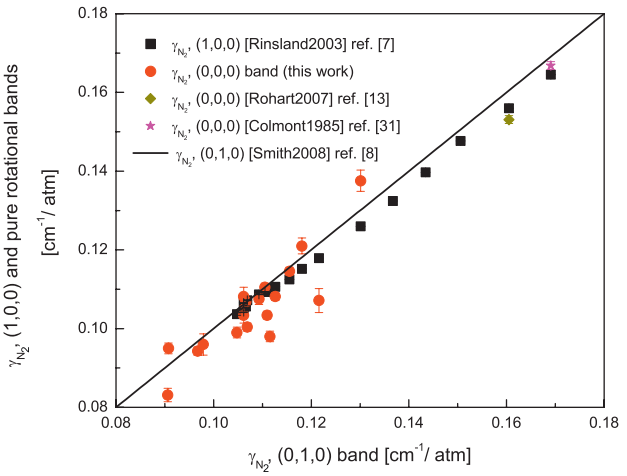

Fig. 10. A comparison of nitrogen-broadened half-widths of *R*-branch lines of HCN from pure rotational, $(1,0,0)$ and $(0,1,0)$ bands. The widths of lines from pure rotational and $(1,0,0)$ bands are plotted against widths of the corresponding $(0,1,0)$ lines.

Therefore either polynomial can be used safely, although the polynomial derived here seems to account slightly better for the widths of pure rotational lines.

Although it was previously suggested that there is no strong vibrational dependence for the foreign gas broadening of HCN lines [3], the observations of Figs. 7–9 suggest the possibility of such a dependence. In Fig. 10 the N_2-broadened half-widths (*R*-branches) from $(1,0,0)$ [7], $(0,1,0)$ [8] and pure rotation bands measured here and in [13,31] are compared. The half-widths of $(0,1,0)$ band are taken as reference values. It seems that the values from $(1,0,0)$ and $(0,1,0)$ bands are a little different at lower *J*'s (wider widths). Unfortunately, there is not enough experimental information to study the vibrational dependence for the oxygen broadening.

7. Conclusion

The construction of a CW-THz spectrometer based on two ECDL has allowed the HCN-broadening coefficients for oxygen and nitrogen to be measured at frequencies from 532 GHz to 3.26 THz ($5 \leqslant J \leqslant 36$). The correct operation of this newly constructed instrument was validated by the good agreement between the measured nitrogen data and that published by Sergent-Rozey et al. [9]. The oxygen-broadening coefficients were computed as a function of the rotation quantum number using the semiclassical RBE formalism for various parameterizations of the isotropic part of the interaction potential which governs the relative molecular motion and influences significantly the theoretical linewidth values. Although all tested parameterizations provided a reasonable agreement with the experimental data, the Viso1 set of parameters was retained

as optimal. Since the application of the measured data to the air-broadening parameter tabulated in the HITRAN database displayed a significant discrepancy for $|m|>29$, a new fourth-order polynomial was therefore suggested for inclusion in HITRAN to improve the accuracy for these transitions. Comparison between the data measured for nitrogen broadening with the $(1,0,0)$ and $(0,1,0)$ bands recorded in the infrared region indicated the possibility of a vibrational dependency; further investigations are required in order to confirm this tendency.

Acknowledgments

The authors would like to thank J.F. Lampin and K. Blary of the IEMN for the fabrication of the photomixer devices, along with Marc Fourmentin for his assistance in the preparation of this article. The authors also thank M.A.H. Smith for her comments regarding this work. This work was partially funded by Agence De l' Environnement et de la Maîtrise de l'Energie (ADEME), the Région Nord–Pas de Calais, the European Commission and the Délégation Générale pour l'Armement (projet de Recherche Exploratoire et Innovation no. 06.34.037). The Laboratoire de Physico-Chimie de l'Atmosphère and the Laboratoire de Physique des Lasers, Atomes et Molecules participate in the Centre d'Etudes et de Recherches Lasers et Applications (CERLA).

References

[1] Teanby NA, Irwin PGJ, de Kok R, Vinatier S, Bézard B, Nixon CA, et al. Vertical profiles of HCN, HC_3N, and C_2H_2 in Titan's atmosphere derived from Cassini/CIRS data. Icarus 2007;186:364–84.
[2] Kim SJ, Geballe TR, Noll KS, Courtin R. Clouds, haze, and CH_4, CH_3D, HCN, and C_2H_2 in the atmosphere of Titan probed via 3 μm spectroscopy. Icarus 2005;173:522–32.
[3] Rothman LS, Jacquemart D, Barbe A, Benner DC, Birk M, Brown LR, et al. The HITRAN 2004 molecular spectroscopic database. JQSRT 2005;96:139–204.
[4] Weisstein EW, Serabyn E. Submillimeter line search in Jupiter and Saturn. Icarus 1996;123:23–36.
[5] Devi VM, Benner DC, Smith MAH, Rinsland CP, Predoi-Cross A, Sharpe SW, et al. A multispectrum analysis of the ν_2 band of $H^{12}C^{14}N$: Part I. Intensities, broadening, and shift coefficients. J Mol Spectrosc 2005;231:66–84.
[6] Devi VM, Benner DC, Smith MAH, Rinsland CP, Sharpe SW, Sams RL. A multispectrum analysis of the $2\nu_2$ spectral region of $H^{12}C^{14}N$: intensities, broadening and pressure-shift coefficients. JQSRT 2004;87:339–66.
[7] Rinsland CP, Devi VM, Smith MAH, Benner DC, Sharpe SW, Sams RL. A multispectrum analysis of the ν_1 band of $H^{12}C^{14}N$: Part II. Air- and N_2-broadening, shifts and their temperature dependences. JQSRT 2003;82:343–62.
[8] Smith MAH, Rinsland CP, Blake TA, Sams RL, Benner DC, Devi VM. Low-temperature measurements of HCN broadened by N_2 in the 14 μm spectral region. JQSRT 2008;109:922–51.
[9] Sergent-Rozey M, Nguyen-Van-Thanh, Rossi I, Bouanich JP. Nitrogen broadening measurements in the far infrared-spectrum of HCN. J Mol Spectrosc 1990;142:182–90.
[10] Schmidt C, Lambot D, Walrand J, Blanquet G, Bouanich JP. Diode-laser measurements of N_2-broadening coefficients in the ν_2 band of HCN. J Mol Spectrosc 1992;151:292–302.
[11] Schmidt C, Populaire JC, Walrand J, Blanquet G, Bouanich JP. Diode-laser measurements of N_2-broadening coefficients in the ν_2 band of HCN at low-temperature. J Mol Spectrosc 1993;158:423–32.
[12] Robert D, Bonamy J. Short-range force effects in semi-classical molecular line broadening calculations. J Phys—Paris 1979;40:923–43.
[13] Rohart F, Nguyen L, Buldyreva J, Colmont JM, Wlodarczak G. Lineshapes of the 172 and 602 GHz rotational transitions of $HC^{15}N$. J Mol Spectrosc 2007;246:213–27.
[14] Buldyreva J, Bonamy J, Robert D. Semiclassical calculations with exact trajectory for N_2 rovibrational Raman linewidths at temperatures below 300 K. JQSRT 1999;62:321–43.
[15] Landau LD, Lifshitz EM. Course of theoretical physics. Oxford: Pergamon; 1976.
[16] Hindle F, Cuisset A, Bocquet R, Mouret G. Continuous-wave terahertz by photomixing: applications to gas phase pollutant detection and quantification. CR Phys 2008;9:262–75.
[17] Matton S, Rohart F, Bocquet R, Mouret G, Bigourd D, Cuisset A, et al. Terahertz spectroscopy applied to the measurement of strengths and self-broadening coefficients for high-J lines of OCS. J Mol Spectrosc 2006;239:182–9.
[18] Chen P, Pearson JC, Pickett HM, Matsuura S, Blake GA. Measurements of $^{14}NH_3$ in the $\nu_2=1$ state by a solid-state, photomixing, THz spectrometer, and a simultaneous analysis of the microwave, terahertz, and infrared transitions between the ground and ν_2 inversion-rotation levels. J Mol Spectrosc 2006;236:116–26.
[19] Mouret G, Matton S, Bocquet R, Hindle F, Peytavit E, Lampin JF, et al. Far-infrared cw difference-frequency generation a using vertically integrated and planar low temperature grown GaAs photomixers: application to H_2S rotational spectrum up to 3 THz. Appl Phys B 2004;79:725–9.
[20] Podobedov VB, Plusquellic DF, Fraser GT. THz laser study of self-pressure and temperature broadening and shifts of water vapor lines for pressures up to 1.4 kPa. JQSRT 2004;87:377–85.
[21] Bigourd D, Cuisset A, Hindle F, Matton S, Bocquet R, Mouret G, et al. Multiple component analysis of cigarette smoke using THz spectroscopy, comparison with standard chemical analytical methods. Appl Phys B 2007;86:579–86.
[22] Humlicek J. Optimized computation of the Voigt and complex probability functions. JQSRT 1982;27:437–44.
[23] Jorgensen UG, Almlof J, Gustafsson B, Larsson M, Siegbahn P. CASSCF and CCI calculations of the vibrational band strengths of HCN. J Chem Phys 1985;83:3034–42.
[24] Gray CG, Gubbins KE. Theory of molecular fluids. Fundamentals, vol. 1. London/New York: Oxford University Press (Clarendon Press); 1984.
[25] Stogryn DE, Stogryn AP. Molecular multipole moments. Mol Phys 1966;11:371–93.
[26] Rohart F, Derozier D, Legrand J. Foreign gas relaxation of the $J=0->1$ transition of $HC^{15}N$. A study of the temperature-dependence by coherent transients. J Chem Phys 1987;87:5794–803.
[27] Johnston HL, McCloskey KE. Viscosities of several common gases between 90 K and room temperature. J Phys Chem 1940;44:1038–58.
[28] Tsao CJ, Curnutte B. Line-widths of pressure-broadened spectral lines. JQSRT 1962;2:41–91.
[29] Hietanen J, Jolma K, Horneman VM. The infrared calibration lines of HCN in the region of ν_2 with the resolution of 0.003 cm^{-1}. J Mol Spectrosc 1988;127:272–4.
[30] Herzberg G. Spectra of diatomic molecules. Princeton: Van Nostrand; 1966.
[31] Colmont JM. Collisional broadening of the $J=1<-0$ transition of $HC^{15}N$ by nitrogen, oxygen, helium, and air. J Mol Spectrosc 1985;114:298–304.

[32] Kaghat F. Profils des transitions millimétriques : Analyse par spectroscopie résolue en temps du rétrécissement et de l'asymétrie liés à la distribution des vitesses moléculaires. Ph.D. thesis, Université de Lille 1,1995.
[33] Trautz M, Melster A. Die reibung, wärmeleitung und diffusion in gasmischungen XI. Die reibung von H_2, N_2, CO, C_2H_4, O_2 und ihren binären gemischen. Ann Phys 1930;399:409–26.
[34] Lemaire V, Babay A, Lemoine B, Rohart F, Bouanich JP. Self- and foreign-gas-broadening and shifting of lines in the v_2 band of HCN. J Mol Spectrosc 1996;177:40–5.